FINAL FOCUS SYSTEMS FOR LINEAR COLLIDERS*

ROGER A. ERICKSON

Stanford Linear Accelerator Center,
Stanford, California 94305

TABLE OF CONTENTS

FINAL FOCUS SYSTEMS FOR LINEAR COLLIDERS

Roger A. Erickson

Stanford Linear Accelerator Center
Stanford, California 94305

1. INTRODUCTION

The final focus system of a linear collider must perform two primary functions: it must focus the two opposing beams so that their transverse dimensions at the interaction point are small enough to yield acceptable luminosity, and it must steer the beams together to maintain collisions. In addition, the final focus system must transport the outgoing disrupted beams to a location where they can be recycled or safely dumped. As of this writing, the only full-scale collider final focusing system actually constructed is that of the SLAC Linear Collider, better known simply as the SLC.

The SLC is designed to collide 50 GeV beams of electrons and positrons at an initial luminosity of about 10^{29} cm^{-2} sec^{-1} and ultimately to reach a luminosity of 6×10^{30} cm^{-2} sec^{-1} when several planned improvements are completed.[1] While this luminosity is appropriate for the SLC energy range, a linear collider built for a much higher energy will need much greater luminosity. This is because the cross sections for interesting physics, described by point-like fundamental processes, drop with increasing center-of-mass energy as $1/E_{\rm cms}^2$. The cross section for producing new quark-antiquark states, for example, is expected to be roughly

$$\sigma_{Q\overline{Q}} \approx 10^{-37} \, E_{\rm cms}^{-2} \, [\text{TeV}^{-2}] \, \text{cm}^2 \quad . \tag{1}$$

Thus, the luminosity appropriate for a machine with energy $E_{\rm cms}$ is about

$$\mathcal{L} = 10^{33} \, E_{\rm cms}^2 \, [\text{TeV}^2] \, \text{cm}^{-2} \, \text{sec}^{-1} \quad . \tag{2}$$

At this luminosity, roughly 10 $Q\overline{Q}$ states would be produced per day if they exist at all at that energy. The event rate for interesting physics processes is expected to be about the same for all machines satisfying this relationship.[2]

Luminosity is given by the expression

$$\mathcal{L} = \frac{1}{4\pi} \frac{f \, N^+ \, N^-}{\sigma_x \sigma_y} \tag{3}$$

where N^+ and N^- are the numbers of positrons and electrons per bunch, and f is the frequency of collisions. σ_x and σ_y are the RMS radii of the bunches in the horizontal and vertical dimensions,

respectively, and are given in lowest order by

$$\sigma = \sqrt{\frac{\epsilon_N \beta^*}{\gamma}} \qquad (4)$$

where ϵ_N is the normalized emittance, β^* is the value of the betatron function at the collision point and $\gamma = E/m_e c^2$. Thus, for identical round beams,

$$\mathcal{L} = \frac{1}{4\pi} \frac{f N^2}{\beta^*} \frac{\gamma}{\epsilon_N} \quad . \qquad (5)$$

Luminosity increases linearly with energy if all other machine characteristics can be held constant, because the effective emittance shrinks as the longitudinal momentum increases.

To reach collision energies much higher than the SLC while maintaining the luminosity implied by Eq. (2) requires some fundamental improvement in the design. This may be an increase in bunch population N or the repetition rate f, either of which increases the average beam power and the electric bill, or a decrease in ϵ_N or β^*. The prospects for reducing ϵ_N below 3×10^{-5} rad m (the SLC design value) are discussed elsewhere.[3]

There are no fundamental limitations to producing very small values of β^*. There are, however, practical limits imposed by the strength, field quality and alignment tolerances of focusing magnets, the space requirements of the experimental detector, and the overall size of the focusing system as limited by the site boundaries. In this paper, the functions of final focus systems in general will be described, along with a discussion of performance limitations arising from some of these practical design considerations. To illustrate the main ideas, the final focus system of the SLC will be presented, and the basis for the key parameter choices will be discussed.

The SLC is not a true linear collider in the sense of having two linacs pointed at each other. Instead, a single linac is used to accelerate bunches of positrons and electrons simultaneously to the desired energy. The bunches are then separated and guided around two arcs of alternating-gradient bending magnets to opposite ends of the final focus system. At the time of this writing, the construction of the SLC has been essentially completed, and initial commissioning tests are in progress. While most of the examples in this paper are drawn from the SLC, the principles and conclusions are generally applicable to other linear collider designs as well.

2. ELEMENTARY OPTICAL CONSIDERATIONS

An arbitrarily small value of β^*, and hence an arbitrarily small focused spot, can be obtained by using sufficiently strong quadrupole magnets close to the interaction point. There are, however, both first-order and higher-order considerations that define limits on β^*, below which

further reductions are useless. Among these limiting considerations are the bunch lengths, the synchronization precision and the momentum spread of the beams. Because of these and other considerations discussed below, the SLC will be operated with a β^* of 4 to 10 mm, depending on how the final focus is set up and tuned.

2.1 Bunch Length

The RMS radius $\sigma(z)$ of a beam near the interaction point is given by:

$$\sigma(z) = \sigma^* \sqrt{1 + \frac{z^2}{\beta^{*2}}} \tag{6}$$

where z is the distance along the beam direction from the point where the minimum radius σ^* occurs. The depth-of-focus scale is set by β^*. If the RMS bunch length σ_z is much greater than β^*, only part of the bunch is in focus at any instant during the collision. The resulting loss in luminosity has been computed for Gaussian bunches (Gaussian in all three dimensions) by integrating over the lengths of both bunches as they pass through each other. Figure 1 shows the relative luminosity as a function of σ_z/β^*.
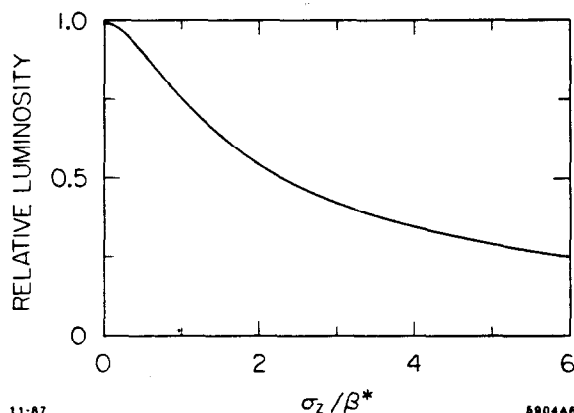

Fig. 1. Luminosity falls with increasing bunch length σ_z. Curve is normalized to β^*.

The RMS bunch length in the SLC is about 1 mm, while the design values of β^* are in the range of 4 to 10 mm. Thus, the bunch-length limit is not yet an issue for the SLC. In a future linear collider, however, this may become a very important consideration. For example, a set of parameters for a 1 TeV center-of-mass linear collider recently suggested by R. Palmer[4] includes $\beta_y^* = 50$ μm, which would require a very short σ_z. Palmer suggested a σ_z of 43 μm for this design.

It should be noted that Eqs. (3) through (6) are strictly accurate only when the densities of the opposing bunches are low enough that they do not disrupt each other. When the bunches are very dense, they experience a mutual focusing force due to the electromagnetic attraction between them.[5] This focusing force, which is sensitive to the bunch lengths, reduces the effective beam size near the interaction point and enhances the luminosity.

4

2.2 Arrival-Time Synchronization

In order to achieve the full potential luminosity with a small β^*, the opposing bunches must arrive at the focal point simultaneously. If the second bunch is late by an amount Δt when the first bunch arrives at the minimum-waist point, the actual collision will occur at a point offset from the desired minimum-waist point by an amount $c\Delta t/2$. Figure 2 shows luminosity loss as a function of this timing error. Controlling the arrival time difference to the necessary precision is easier in the SLC, in which both the e^+ and e^- bunches are accelerated in the same linac, than it might be in a collider built with two separate linacs. In the SLC linac, the e^- bunch trails the e^+ bunch by $168\frac{1}{2}$ S-band buckets, a separation which can be controlled by adjusting the relative r.f. phase of the e^+ and e^- damping rings, which are physically close together and synchronized to the same oscillator. The position of each bunch within its bucket is then determined by monitoring the final energy of each beam. In this way, a reproducible separation can be maintained with a precision of about 1 mm (corresponding to about 3 psec). In the Palmer machine mentioned above, $(\beta_y^* = 50~\mu\text{m})$, two independent linacs would have to be synchronized to a precision of about 150 femtoseconds. Maintaining this level of synchronization over a distance of several kilometers would pose an interesting problem.
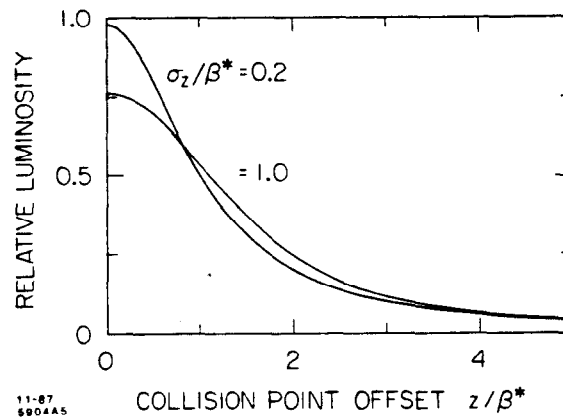
Fig. 2. Luminosity loss as a function of the distance from the collision point to the minimum β point for two bunch lengths. Curves are normalized to β^*.

2.3 Demagnification

A focusing system with a minimum number of components is illustrated schematically in Fig. 3. Here a single thin lens of focal length f is used to form an image at the Interaction Point (IP). The source is a round spot of radius x_1. It can be seen from elementary geometric optics that the condition for bringing an image into focus at the IP is

$$\frac{1}{f} = \frac{1}{L_1} + \frac{1}{L_2} \ .$$

(7)

5

The image size, x_2 is then

$$x_2 = -\left(\frac{L_2}{L_1}\right) x_1$$

$$= -M \, x_1 \tag{8}$$

and

$$\theta_2 = -\frac{1}{M} \, \theta_1 \tag{9}$$

where L_1 and L_2 are the source and image distances from the lens, and their ratio defines the magnification M. For a given total system length, the smallest image is obtained when L_2 is as short as possible and the lens is strong (short f).
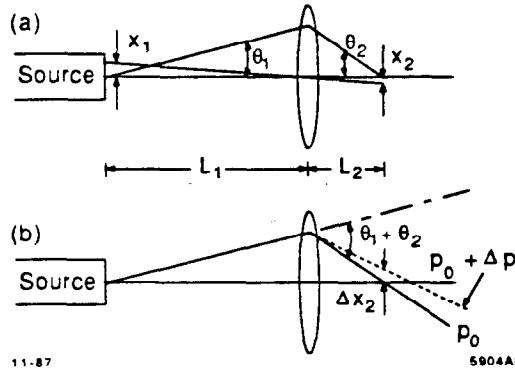

Fig. 3. A thin lens focuser (a). Particles of higher momentum come to a focus downstream of the nominal focal point (b).

The source spot at the input to the SLC final focus (after correction for linear dispersion) has a radius of approximately $x_1 = 50\ \mu$m at a point about 145 m from the IP, with an angular divergence θ_1 of about 6 μrad. Approximating the final set of quadrupole magnets by a thin lens at their common midpoint 5 m from the IP leads to $M = 1/28$, $x_2 = 1.8\ \mu$m and $\theta_2 = 168\ \mu$rad. These results are surprisingly close to the design values for the final spot size of the SLC (cf. Table 1).

The shortcomings of such a simple design become apparent when the finite momentum spread of the beam is considered. A particle near the outer envelope of the beam with momentum higher than the mean beam momentum by a fraction $\Delta p/p$ will be deflected $\Delta\theta/\theta$ less by the lens, as shown in Fig. 3b. Such particles will come to a focus at a point downstream of the nominal IP, resulting in a larger, defocused spot at the point where they collide with the opposing beam.

$$\Delta x_2 \approx L_2 \, \Delta\theta$$

$$\approx L_2 \left(1 + \frac{1}{M}\right) \theta_1 \, \frac{\Delta p}{p} \, . \tag{10}$$

6

The actual spot size at the collision point will be the quadratic sum of the "geometric spot size" and this "chromatic spot size."

$$\sigma_x^2 = M^2 x_1^2 + \left[L_2(1 + \frac{1}{M}) \, \theta_1 \, \frac{\Delta p}{p} \right]^2 \quad , \tag{11}$$

where x_1 and θ_1 are now considered the RMS width and angular spread of the input beam. A momentum spread of 0.5% increases the final spot to $\sigma_x = 4.7 \ \mu m$ in the previous example. This is substantially larger than the pure geometric size and reduces the luminosity by a factor of seven compared to the "monochromatic" calculation.

For fixed L_2 there is an optimum value of M, below which there is no improvement in actual final spot size. Differentiating Eq. (11) with respect to M gives a minimum spot size when

$$\frac{\sqrt{M+1}}{M^2} = \frac{1}{L_2 \frac{\Delta p}{p}} \frac{x_1}{\theta_1} \quad . \tag{12}$$

In the example above, this occurs when $M \approx 1/18$, and results in $\sigma_x = 4.0 \ \mu m$.

Substituting

$$\beta^* = M^2 \frac{\sigma_{x_1}}{\sigma_{\theta_1}} \tag{13}$$

in Eq. (12) gives the optimum β^* for the thin-lens system:

$$\beta^* = \sqrt{1+M} \, L_2 \, \frac{\Delta p}{p} \quad . \tag{14}$$

Since M is small but always positive, and L_2 is greater than or equal to f, it follows that

$$\beta^* \geq f \, \frac{\Delta p}{p} \tag{15}$$

for any final focus system without chromatic correction features. Unless some exotic[6] new focusing technique is employed, the focal length f is limited by magnet technology and mechanical interference near the experimental detector. The minimum possible spot size is then determined by the momentum spread of the accelerator.

For more complicated examples, it is convenient to use TRANSPORT[7] notation, in which optical elements and drifts are represented by matrices, and a particle trajectory can be represented by a six-element vector[8] $\mathbf{x}_i = (x, \theta, y, \phi, \ell, \delta)$. In this notation, $\theta = x'$, $\phi = y'$, ℓ is the deviation in pathlength from the central trajectory, and $\delta = \frac{\Delta p}{p}$. The one-dimensional, monoenergetic thin

lens example can then be represented by:

$$\begin{pmatrix} x_2 \\ \theta_2 \end{pmatrix} = \begin{pmatrix} 1 & L_2 \\ 0 & 1 \end{pmatrix} \begin{pmatrix} 1 & 0 \\ -f^{-1} & 1 \end{pmatrix} \begin{pmatrix} 1 & L_1 \\ 0 & 1 \end{pmatrix} \begin{pmatrix} x_1 \\ \theta_1 \end{pmatrix} \tag{16}$$

which simplifies to

$$\begin{pmatrix} x_2 \\ \theta_2 \end{pmatrix} = R \begin{pmatrix} x_1 \\ \theta_1 \end{pmatrix} \tag{17}$$

where R is the first-order matrix

$$R = \begin{pmatrix} (1 - L_2 \, f^{-1}) & (L_1 + L_2(1 - L_1 \, f^{-1})) \\ -f^{-1} & (1 - L_1 \, f^{-1}) \end{pmatrix} . \tag{18}$$

Focusing implies $R_{12} = 0$, i.e., the position of a particle at the end is independent of its angle at the beginning. Setting this element to zero gives Eq. (7). Then

$$R = \begin{pmatrix} -M & 0 \\ -(\frac{1}{L_1} + \frac{1}{L_2}) & -\frac{1}{M} \end{pmatrix} \tag{19}$$

where again $M = \frac{L_2}{L_1}$.

To see the effect of a finite momentum spread, replace f by $(f + \triangle f) = f(1 + \delta)$ in Eq. (18) above. $\triangle f / f$ is a small fractional change in focal length due to a small fractional change δ in momentum. To simplify the algebra, define $d = \delta/(1 + \delta)$. Then f^{-1} is replaced by $f^{-1}(1 - d)$, and the resulting matrix is designated R'. Note that $d = \delta$ in the limit of $\triangle p \ll p$. With this substitution, Eq. (18) becomes:

$$R' = \begin{pmatrix} -M + (M+1)d & L_2(1 + \frac{1}{M})d \\ -f^{-1}(1-d) & (1 - L_1 f^{-1}) + L_1 f^{-1} d \end{pmatrix} . \tag{20}$$

With this substitution, R'_{11} becomes $-M + (M+1)d$, the original part plus a term proportional to momentum spread. In the language of TRANSPORT, the monoenergetic part, $-M$, is R_{11}, and the second part is identified as the second-order term T_{116} times d. Similarly, R'_{12} picks up a non-zero part $L_2(1 + \frac{1}{M})$ which multiplies d and is identified as the T_{126} term [cf. Eq. (10)]. Thus,

$$x_2 \approx R_{11} x_1 + T_{116} \, x_1 \, d + T_{126} \, \theta_1 \, d . \tag{21}$$

In this example, the identification of these second-order coefficients as the T_{116} and T_{126} TRANSPORT terms is an approximation that is strictly correct only in the limit of small $\triangle p$ as d approaches δ.

A more complicated system will have additional terms in this series. The general form of the series expansion for the ith element of the x-vector is:

$$x_i = \sum_j R_{ij} \, x_j + \sum_j \sum_k T_{ijk} \, x_j \, x_k$$

$$+ \sum_j \sum_k \sum_m U_{ijkm} \, x_j \, x_k \, x_m \tag{22}$$

$$+ \text{ higher order terms } .$$

The goal in designing any final focus system is to make the magnification terms, R_{11} in the x dimension and R_{33} in the y dimension, small enough to give the desired spot size, while keeping all other terms negligibly small. In this example, the first-order magnification is $R_{11} = -M$, and R_{12} is identically zero at the focal point. The second-order term $T_{116}x\delta$ is negligible, but $T_{126}\theta\delta$ is large and dominates the final spot size. In realistic examples with thick quadrupole lenses, this is still generally true; the T_{126} term dominates the final spot size unless specific features are included to cancel it. It is assumed throughout this paper that any final focus system will be built with mid-plane symmetry, i.e., that all xy coupling terms will be zero.

2.4 Telescopes

The properties of a simple optical telescope can be shown to have direct application to a charged particle transport system. Consider two lenses of focal lengths f_1 and f_2 as shown in Fig. 4. If the spacings are chosen to be $L_1 = f_1$, $L_2 = f_2$ and $L_3 = L_1 + L_2$, then for a monoenergetic beam,

$$R = \begin{pmatrix} -\frac{f_2}{f_1} & 0 \\ 0 & -\frac{f_1}{f_2} \end{pmatrix} = \begin{pmatrix} -M & 0 \\ 0 & -\frac{1}{M} \end{pmatrix} . \tag{23}$$

Comparing to the single lens case, Eq. (19), it can be seen that the R_{21} term has dropped out, i.e., the angle of a particle leaving the system depends only on its angle at the entrance and not on its position.
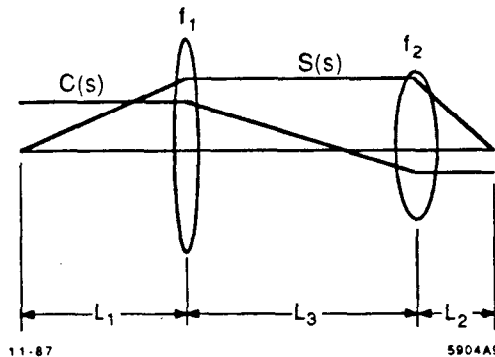

Fig. 4. A telescope constructed with two thin lenses, showing the characteristic sine-like and cosine-like trajectories.

A useful property of telescopes of this kind is that they can "slide" to vary the relative lengths of the leading and trailing drift distances. If the drift length L_1 upstream of the first lens is shortened by an amount $\triangle L_1$, the focal point will move downstream by an amount $\triangle L_2 = -M^2 \triangle L_1$. The first-order R matrix remains unchanged. This property was used to advantage in the design of the final telescope of the SLC, as discussed in Section 4.6 below.

The chromatic properties of a simple telescope can be seen by replacing f_1^{-1} by $f_1^{-1}(1 - d)$ and f_2^{-1} by $f_2^{-1}(1 - d)$ in the matrix for each lens, as in the single lens example. The R-matrix for the complete telescope then becomes:

$$ R' = \begin{pmatrix} -\frac{L_2}{L_1} + \left(\frac{L_3}{L_1}\right) d^2 & L_3(d + d^2) \\ \frac{-L_3}{L_1 L_2} (d - d^2) & -\frac{L_1}{L_2} + \frac{L_3}{L_2} \delta^2 \end{pmatrix} \quad . \tag{24} $$

Comparing to Eq. (20), it can be seen that third-order chromatic terms proportional to d^2 (U_{1166} and U_{2266}) have appeared on the diagonal, but the second-order terms, T_{116} and T_{226}, have vanished. Other third-order contributions (U_{1266} and U_{2166}) have appeared on the off-diagonal terms. T_{126} is unchanged and still the dominant aberration, and the β^* limit in Eq. (15) still applies.

A final focus design based on this simple telescope arrangement was considered briefly for the SLC at an early stage in the design process.[9] A final spot radius of 2μm could be obtained, even with $\triangle p/p = 0.5\%$, by positioning the nearest face of the innermost quadrupole 20 cm from the IP. In this design, the innermost triplet of quadrupoles required magnetic field gradients of 150 kG/cm. It is conceivable that this gradient could be achieved with a quadrupole constructed from $Sm Co_5$ permanent magnets (7.5 kG pole tip fields) at a radius of 0.5 mm. The field quality requirements, and thus the dimensional and magnetic tolerances on the individual pole pieces, would be severe. While it may be practical in a few years, such a magnet is still beyond present technology. Another practical problem is that such a magnet in the SLC would be destroyed by just a few errant beam pulses. This scheme was rejected in favor of an approach based on active cancellation of chromatic aberrations.

3. CHROMATIC ABERRATIONS

3.1 Mathematical Preliminaries

It is useful at this point to define three functions which in combination can describe any trajectory through a given system. These functions, designated $C(s)$, $S(s)$ and $D(s)$, are sometimes called the "cosine-like trajectory," the "sine-like trajectory," and the dispersion function. $C(s)$ is simply the transverse offset of a particle from the central trajectory as it traverses a given system, when it starts with an offset of 1 unit and zero slope at the input ($C(0) = 1$, $C'(0) = 0$). The

value of $C_x(s)$ at any point s along a beam transport system is equal to R_{11} at that point and is simply the magnification. Similarly, a function $C_y(s)$ can be defined for the y-dimension and equals R_{33}. $S(s)$ is the function that starts with zero offset, but a slope of 1, and is equal to R_{12} (in the x-dimension) at each point in the system. At any image point along the way, and in particular at the IP, $R_{12} = 0$. This is a first-order property of any telescopic system.

The dispersion function $D(s)$ relates the position offset to fractional momentum change and is equal at each point to R_{16}. Its value at the focal point can be calculated as an integral over the system:

$$R_{16} = D(s_2) = M \int_{s_1}^{s_2} \frac{S(s)}{\rho} \, ds \qquad (25)$$

where ρ is the radius of curvature of the central trajectory as it passes through any dipole field. R_{16} will be zero at the IP if the dipoles in the system (if there are any) are arranged in such a way that the integral over the whole system is zero. This will be the case, for example, if dipoles are incorporated into the design only in equal-strength pairs 180° apart in betatron phase, i.e., at points where $S(s)$ has equal amplitude but opposite sign.

Each of the T-matrix terms and higher terms can be expressed as integrals over various combinations of these three functions and their derivatives. These integral expressions are derived and tabulated in Reference 10. The three second-order chromatic aberrations in a point-to-point imaging system are T_{116}, T_{166} and T_{126}. T_{116} for a quadrupole focusing array is given approximately by

$$T_{116} \approx M \int C' S' \, ds \quad . \qquad (26)$$

This integral vanishes for a pure telescopic system. For the example in Fig. 4, this is obvious from inspection; one or the other of $C'(s)$ and $S'(s)$ is zero everywhere.

In a real design using sets of thick quadrupoles rather than thin lenses, T_{116} will generally not be identically zero. In the design of the SLC, the pure telescopic conditions were relaxed further to reduce the total length of the final focus system, keeping $R_{11} = 0$, but allowing R_{21} to become significant.[11] With this compromise, T_{116} was still small (≈ 6) but not completely negligible.

The T_{166} term is given by

$$T_{166} \approx -\frac{1}{2} M \int D'^2 S \frac{ds}{\rho} - M \int k_1 S D \, ds + M \int k_2 S D^2 \, ds \quad , \qquad (27)$$

where the three integrals represent the contributions from dipoles, quadrupoles and sextupoles, respectively. k_1 and k_2 are the strengths of the quadrupoles and sextupoles. Since each term contains a first power of $S(s)$, each integral can be made zero by designing the system with appropriate symmetries. The contribution from any section of the system with non-zero D or D' can

be cancelled by adding another identical section 180° downstream. This is shown schematically in Fig. 5 for a system of two half-wave telescopes separated by dipoles. In the SLC final focus design T_{166} is approximately $-1. \times 10^{-4}$ m, which when multiplied by $(\triangle p/p)^2$ makes an insignificant contribution to the final spot size.
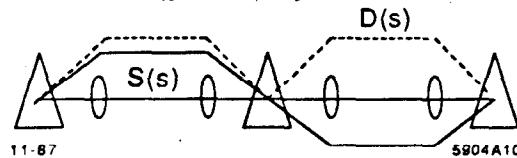

Fig. 5. The T_{166} aberration vanishes in a system of two modules with identical dispersion functions and opposite sine-like trajectories.

The T_{126} term for a point-to-point imaging system is given approximately by

$$T_{126} \approx -M \int S'D'S \frac{ds}{\rho} - M \int S'^2 ds + 2M \int k_2 S^2 D ds \qquad (28)$$

where again the three terms correspond to contributions from dipoles, quadrupoles, and sextupoles, respectively. The dipole term can, in principle, be cancelled exactly by appropriate design, but it is typically small in any case. The quadrupole term being quadratic in S' is always positive and increases in value the more focusing elements are in the system. Note that in a typical design, this term comes mostly from the last quadrupoles, which give the particles large angles (S') as they impinge on the IP. In the final telescope of the SLC, T_{126} is approximately 41 m, considerably larger than the size expected from the thin-lens approximation [Eq. (24)]. This aberration would enlarge the final spot by an order of magnitude if left uncorrected. The key to minimizing the T_{126} contribution is to add sextupoles to the system with strengths k_2 chosen to cancel the first two terms.

3.2 Chromatic Corrections with Sextupoles

To see intuitively how this works, think of a sextupole as a quadrupole with a strength that depends on the radial position of the beam passing through its aperture. The y-component of the field seen by the particles of a beam displaced transversely is given by

$$B_y = B_0 x^2 = B_0 (x_0 + \triangle x)^2 \qquad (29)$$

where x is given by the sum of the position x_0 of the beam centroid and an offset $\triangle x$ of a particular particle from the centroid. Hence,

$$B_y = (2 B_0 x_0)\triangle x + B_0 x_0^2 + B_0 (\triangle x)^2 . \qquad (30)$$

The first term in parentheses corresponds to the position-dependent quadrupole strength. The $B_0 x_0^2$ term represents the net dipole deflection felt by the beam as a whole, and $B_0 (\triangle x)^2$ is a

higher-order term that comes from the fact that the slope of the field is not constant across the geometric width of the beam (as it would be in a true quadrupole field) but increases slightly with increasing $\triangle x$.

Figure 6 shows how the chromatic aberration of a quadrupole can be corrected with a sextupole. A dipole is first used to create linear dispersion. Particles with momentum $p + \triangle p$ are deflected less than those of momentum p, and thus pass through a different part of the sextupole aperture, where they see a stronger focusing field than those on the central trajectory. Of course, the linear dispersion must be removed with one or more dipoles downstream of this point. Sextupoles can be used in this way not only to cancel the chromatic effects of an adjacent quadrupole, but any other quadrupole in the system, either upstream or downstream.
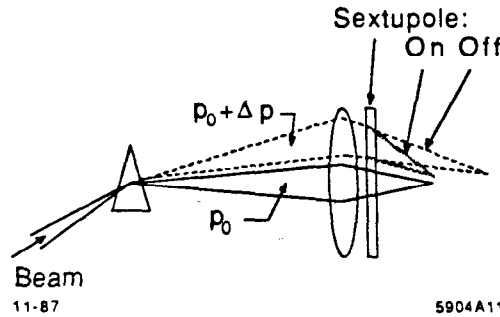

Fig. 6. A dipole and sextupole can be added to a quadrupole focuser to bring off-momentum particles to a focus at the same longitudinal position as the reference beam.

In a quadrupole focusing system without sextupoles, particles with below-nominal momentum come to a focus at a point upstream of the nominal IP; those with higher momentum come to a focus downstream. In a system with sextupoles, the strengths can be chosen to bring a range of momenta to a focus at a single position or even to overcorrect and bring the higher momentum particles to a focus upstream of the nominal image point. This overcorrection can be done in a special Chromatic Correction Section (CCS) upstream of the Final Telescope (FT), compensating in advance for the chromatic aberrations of the final quadrupoles. Specifically, if

$$M \ T_{126}(CCS) = \ T_{126}(FT) \tag{31}$$

then the T_{126} term for the combined system will vanish. In the final telescope of the SLC, $M = 1/5$ and $T_{126}(CCS) \approx 41$ m. The chromatic correction section alone, with the sextupoles turned off, has $T_{126}(CCS) \approx -83$ m. With the sextupoles turned on, $T_{126}(CCS) \approx 205$ m. The net value of T_{126} for the combined system has been calculated to be less than 10^{-4} m.

While T_{126} could be cancelled using only a single sextupole, this would introduce two new problems. These are caused by the second and third terms in Eq. (30): the "even order" terms, so called because they multiply even powers of Δx. The $B_0 x_0^2$ term, which is simply the dipole component of the field seen by the off-axis beam in the sextupole, would steer the beam sideways and introduce linear dispersion. The third term, which varies quadratically across the geometric width of the beam, introduces a geometric aberration, i.e., particles with the same momenta would be focused more or less strongly depending on their transverse positions in the beam. Both problems can be solved by using two sextupoles positioned 180° apart, in two identical half-wave telescopes, as shown in Fig. 7. With this arrangement, the effects produced by the even-order terms of the two sextupoles cancel, while the odd terms (needed to cancel the T_{126} aberration) add.
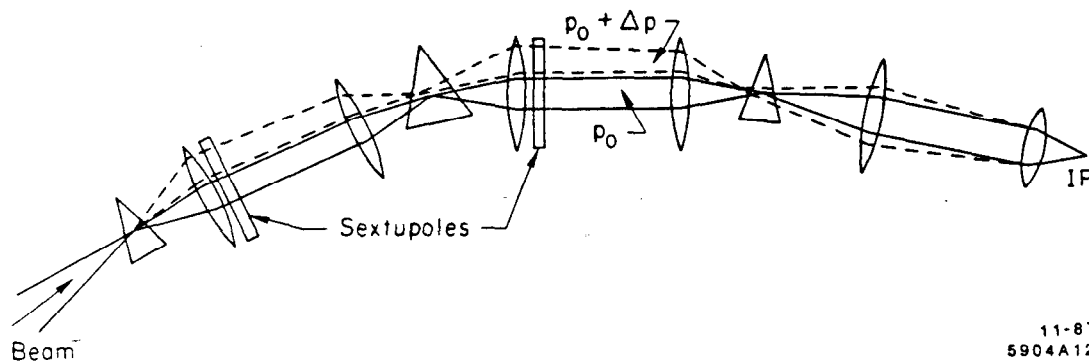

Fig. 7. Two telescopic modules with sextupoles can compensate for the chromatic aberrations of a strong final telescope.

The discussion up to this point has been limited to the x-dimension. The corresponding aberration in the y-dimension, T_{346}, must be cancelled as well. In general, this would require at least one additional pair of sextupoles. One way to do this would be to use two complete chromatic correction sections on each side of the final focus; one pair of half-wave telescopes with sextupoles adjusted to cancel the T_{126} aberration of the complete system, and another pair to take out the T_{346} aberration. In designing the SLC, it was found that both tasks could be done by a single pair of telescopes on each side, but laced with four sextupoles in each telescope, one adjacent to each quadrupole. The odd-numbered sextupoles (counting in the beam direction) are located at points where β_x is larger than β_y and, thus, couple more strongly to the T_{126} term, while the even-numbered sextupoles are located where they couple more strongly to T_{346}. Note that the number of sextupoles in the SLC is twice the minimum number suggested by the discussion above. This came about because the interlacing of the two families of sextupoles introduces higher-order aberrations which would otherwise drop out. By using the additional pairs, it was possible to minimize these other detrimental effects while still cancelling both T_{126} and T_{346} in the space of a single pair of half-wave telescopes.

14

3.3 Third–Order Aberrations

If a system is chromatically corrected to second order, then the third-order aberrations introduced by the sextupoles become the principal source of the residual optical distortions limiting the system's performance. The ratios of the third-order chromatic aberrations to the third-order geometric aberrations are functions of the strengths of the dipoles used for the second-order chromatic corrections. By adjusting the dipole and sextupole strengths in inverse proportions, the total third-order optical distortion can, in general, be minimized without disrupting the second-order chromatic correction. This minimum value occurs when the angular dispersion introduced by the dipoles is approximately equal to the geometric (monoenergetic) angular spread in the beam. This is expressed by the equation:

$$D'_x \frac{\Delta p}{p} = \sqrt{\frac{\epsilon}{\beta_D}} \tag{32}$$

where D'_x is the angular dispersion introduced by the dipole, and β_D is the value of β_x at the dipole. The final adjustment of the strengths of the dipoles is done empirically with computer simulations, observing the final spot for various combinations of magnet strengths and spacings.

Another factor that must be considered when designing a chromatic correction system is the emittance growth that will occur in the dipoles due to fluctuations in the synchrotron radiation. This emittance growth is related to the energy E, the magnet length L, and the bending radius ρ as follows

$$\frac{\Delta\epsilon}{\epsilon} \propto \frac{A}{\epsilon} \frac{E^5}{\rho^5} L^4 \tag{33}$$

where A is a factor that depends on the properties of the beam. The strong dependence on the dipole parameters drives the design to small deflection angles and thus to a long system with strong sextupoles.

As a practical matter, any linear collider must fit within the boundaries of the laboratory. In the case of the SLC, the final focus system was constrained to fit in a section of tunnel approximately 300 m long. This led to a design in which the sextupoles were chosen to be as strong as could be achieved with a conservatively large aperture and conventional iron construction. The total length of each chromatic correction section is about 60 m. While these constraints did not significantly affect the luminosity in the overall system, they did lead to inconvenient mechanical designs in a few places where beamline components were packed closely together. The total loss of luminosity due to emittance growth in these dipoles is about 15%.[11]

In addition to the third-order effects due to the sextupoles, there are third-order effects inherent in the telescopic modules. It was shown above that the effective β^* cannot be less than $f \frac{\Delta p}{p}$ [Eq. (15)] unless some mechanism for cancelling the second order chromatic aberrations

is included in the design. This analysis can be taken a step further to get a rough estimate of the limiting third-order aberration. In the case of the simple telescope (Section 2.4), the largest third-order contribution to the final spot size is U_{1266} [Eq. (24)]. From this it follows that

$$\beta^* \geq f \left(\frac{\Delta p}{p}\right)^2 \quad . \tag{34}$$

This sets the lower limit on β^* for telescopic systems with perfect second-order corrections. It is instructive to consider, as an example, the final telescope of the SLC. With $\frac{\Delta p}{p} = 0.5\%$ and $f \approx 4$ m, this particular third-order effect would become dominant for $\beta^* \approx 100$ μm. It is interesting to note that this particular example sets a limit on β^* that is far below the chosen β^* for the SLC but is twice the β^* suggested in recent design studies for a 1 TeV machine.[4]

In any high-energy final focus design, as elements are added to cancel aberrations of any given order, they will generally introduce other aberrations of higher orders. In the SLC design, the dominant second-order aberrations, T_{116}, T_{166} and T_{126} (and their counterparts in the y dimension) can be reduced to very small levels, leaving third-order aberrations that ultimately limit the performance of the system. In the case of the SLC, the dominant chromatic aberrations are U_{1266} and U_{3466} which cause about a 20% loss in the ultimate luminosity. The dominant geometric aberrations are U_{1222} and U_{3442} which cause about a 10% loss in luminosity.[11] In principle, aberrations of any order can be cancelled by introducing appropriate nonlinear elements in the system; however, no practical scheme has been invented for cancelling aberrations above second order without introducing larger higher-order effects. Ideas that have been considered for cancelling third-order effects typically require excessive magnet strengths or unfeasible alignment tolerances.

3.4 The Optimum Design

There is no unique final focus design that is well-suited for all possible linear colliders. The optimum architecture, as well as the detailed parameters of the design, will depend on the energy, energy spread, emittance and bunch lengths of the beams. A design that is optimized for one set of beam parameters cannot generally be scaled to a much higher energy, even if the other parameters are the same, because of technical limitations. Magnetic field strengths in particular are limited by the maximum attainable current densities in electrical conductors and the magnetic properties of materials and cannot be scaled up to arbitrarily high values.

The use of flat, rather than round, beams is an interesting option for large TeV-class linear colliders. Flat beams are usually mentioned in the context of beamstrahlung radiation, as a way of reducing the spread of collision energies for a given luminosity by reducing the amount of energy lost as electromagnetic radiation.[12] Flat beams also have interesting implications for the optical design of a final focus system. If the system is designed to cancel only the aberrations that enlarge

the vertical beam size, while ignoring horizontal effects, a simpler system with fewer elements is possible, and some aberrations that would otherwise arise from the interplay of these various elements will never appear. Furthermore, quadrupole fields, which are intrinsically asymmetric in the x and y dimensions, can be used to best advantage in arrays that do not require round beams. For fixed field strengths, a smaller, sharper focus can be achieved in one dimension than is possible for a round beam, but at the expense of the other dimension. Whether or not this is a sensible approach for a particular collider depends on the emittance and energy spread of the beams and the details of the final focus system. An interesting example of a 1 TeV flat beam design is given in Reference 13.

4. DESIGN OF THE SLC FINAL FOCUS

4.1 The Design Process

The optical design of the SLC final focus system started with an overall architecture suggested by Karl Brown. The magnet strengths and positions were initially chosen based on a combination of analytic calculations and reasonable guesses. The final design evolved over a period of many months as the implications of various parameter choices were studied and impractical options were discarded. Most of this work was done with the aid of the computer programs TRANSPORT[7] and TURTLE.[14]

TRANSPORT is a second-order matrix multiplication program for designing the first and second-order optics of a proposed system. It has a fitting feature which is used to determine the magnet strengths required to achieve the desired optical and geometric properties of the system. TURTLE is a ray-tracing program that uses the second-order matrices from TRANSPORT to represent each element of the system. Individual rays are traced through each element separately so that higher-order cross coupling effects between elements are included. This program was especially useful for evaluating the severity of the third and fourth-order cross coupling effects introduced by the interleaved sextupole families in the SLC. The results are displayed in the form of histograms which show the density distribution of rays as a function of any of the phase space coordinates.

At an early stage in the SLC project, it was recognized that the final focus system should be designed to accommodate variations in the last telescope. It was anticipated that shorter-focal-length quadrupole lenses would eventually become available, and that the final focus system should be able to exploit any such developments with minimal changes to existing hardware. Ideally, such changes in the final telescope should not require any changes to the other optical modules. Two designs for the final telescope have been developed. Conventional iron quadrupoles have been built for the commissioning and initial operation because of their simplicity and relatively low cost. In parallel with this effort, a design based on superconducting quadrupoles has been developed.[15]

There are two reasons for upgrading the SLC final focus with superconducting quadrupoles. The first is that with higher gradient quadrupoles, a luminosity improvement of roughly a factor of two is possible over the initial machine configuration. The second reason is that superconducting quadrupoles can be operated inside the experimental detector, immersed in a 6 kG solenoid field. This becomes especially important when the SLD,[16] a large second-generation detector, is brought into the SLC.

The final optical design is illustrated in Fig. 8. The β and η functions are plotted in Fig. 9. Each side consists of five half-wave modules: an azimuthal bending section that immediately follows the arc and cancels the off-energy function, η, a telescopic β-matching section that accommodates the extraction system for the outgoing beam, two modules which together correct
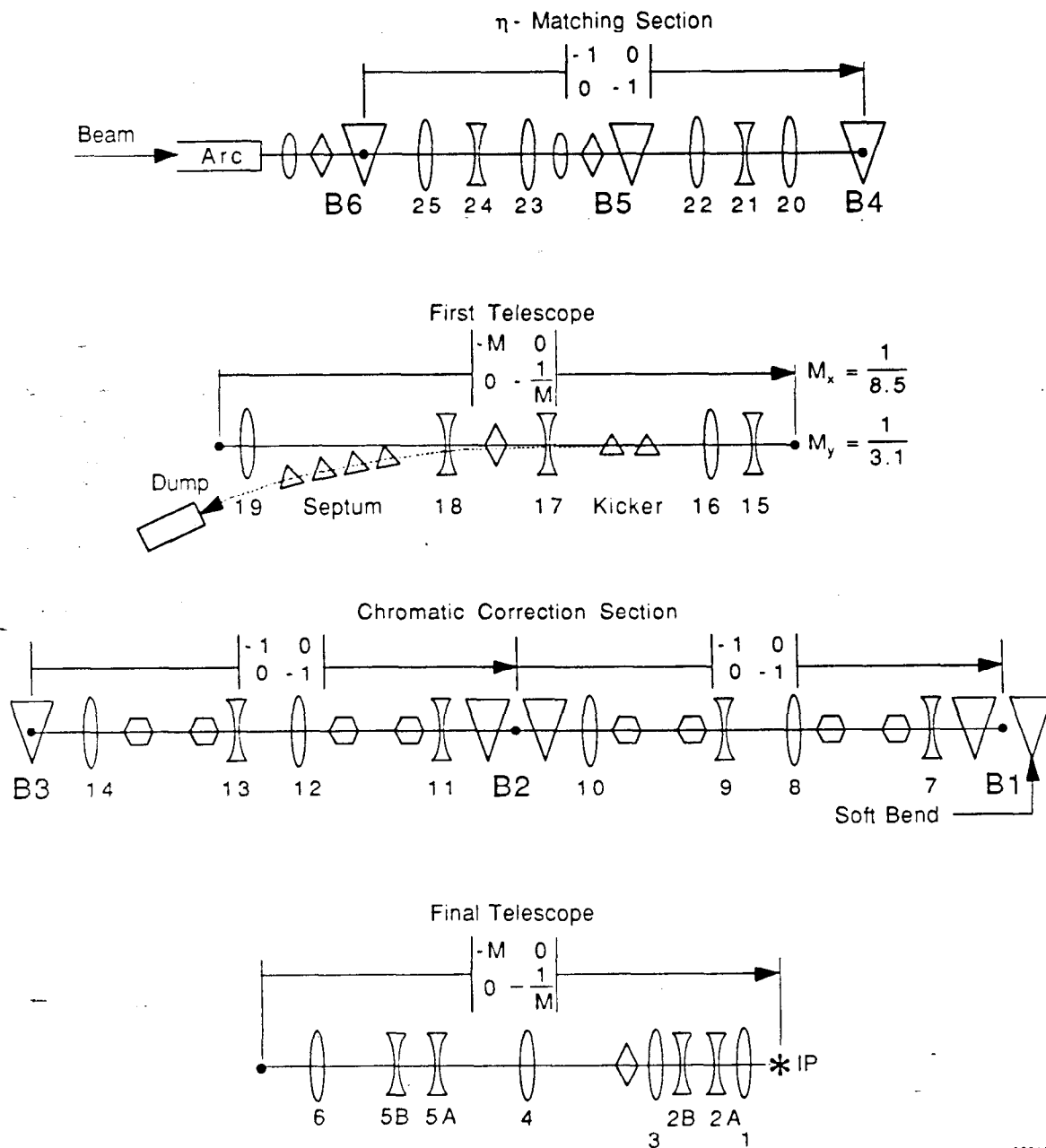
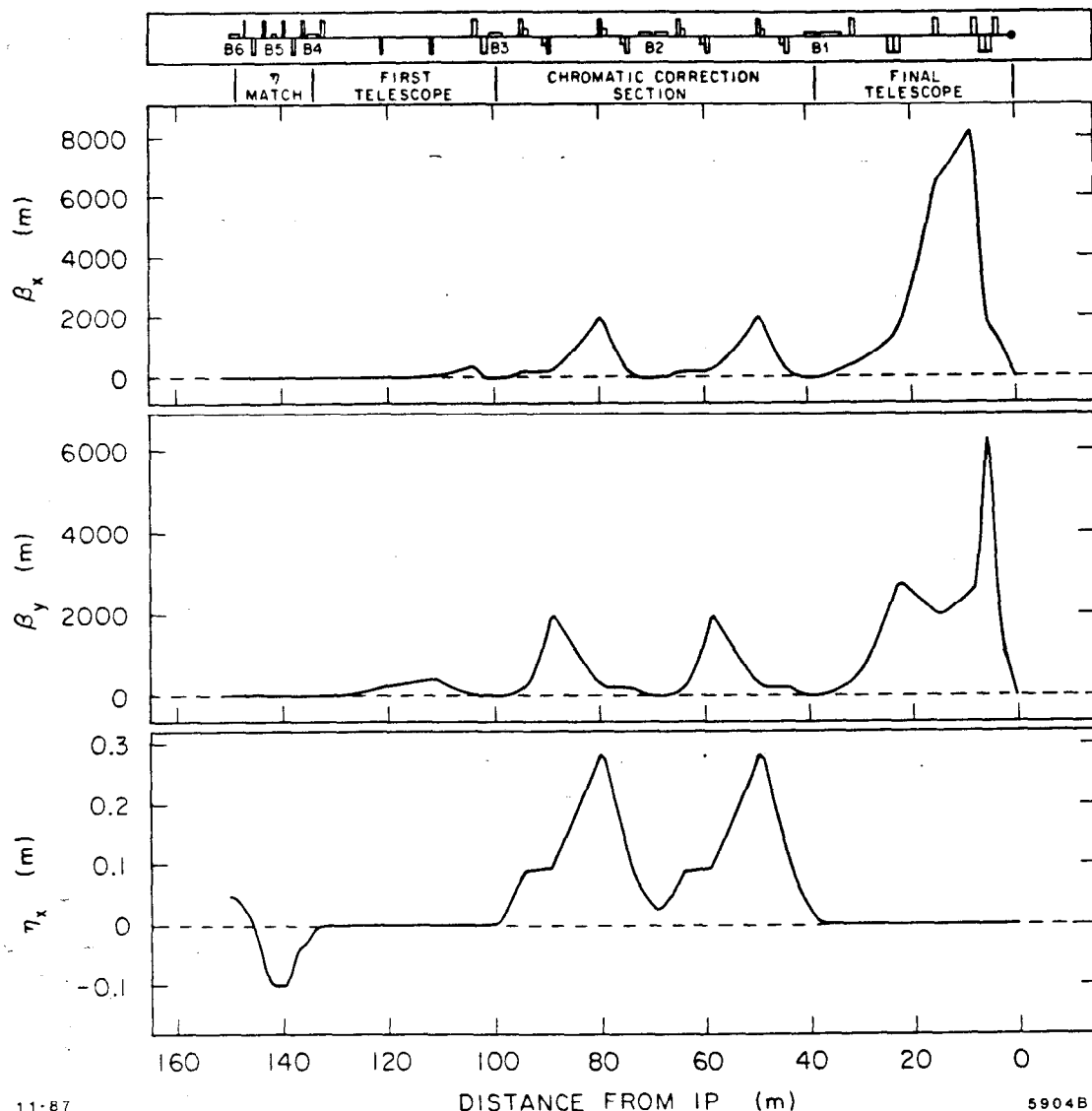Fig. 8. The optical design of the SLC final focus system.

Fig. 9. β and η functions of the SLC final focus. The η function in the y-dimension (not shown) is zero everywhere.

the second-order chromatic distortion of the system, and finally a telescope which demagnifies the beam to the final spot size and provides for fast precise steering.

4.2 The η-Matching Section

Beginning at the end of the arc, the first half-wave module consists of three dipoles separated by quadrupole triplets. The quadrupoles were made strong (0.50 inch full aperture, 8.22 kG pole tip fields) to minimize the total length of this section. The strength of the middle dipole, B5, was chosen so that its momentum dispersion cancels the residual η from the arcs (about 47 mm) by zeroing the η' at the quarter-wave point. The first and third dipoles, B6 and B4, are identical and separated by a half wavelength. Thus, the additional dispersion introduced by B6 is exactly cancelled by B4. Because of the terrain-following feature of the arcs, the beam enters the final focus system pitched up about 0.10°, and with the beam ellipse rolled "inward" a few degrees,

i.e., with the y-axis rolled toward the center of the arcs. The net bend of this module, which is oriented in the plane of the last arc magnet, has a vertical component that brings the beam into the horizontal plane of the IP and a horizontal component that aligns the dispersion-free beam with the first telescopic transformer.

4.3 The First Telescope and Extraction System

Following the η-matching section is a telescopic module, consisting of quadrupoles Q15 through Q19, with demagnifications $1/M$ of 8.51 and 3.09 in the x and y planes, respectively. These values were chosen to transform the elliptical beam at the end of the arc to a round beam with $\sigma_x = \sigma_y \approx 6.0 \ \mu$m at the beginning of the chromatic correction section. Because the envelope of the incoming beam is a rotated ellipse in the xy plane, the magnets in this section must be mounted with a slight roll (approximately 4.1° on the north side, 5.9° on the south). Since the beam leaving this section is circular, all downstream elements are oriented with a vertical y axis.

This module was designed with drift spaces long enough to accommodate the extraction magnets for the outgoing beam. The space between quadrupoles Q16 and Q17 (≈ 7.3 m) accommodates the pulsed kicker. Located 107 m from the IP, the kicker must turn on after the incoming beam has passed and reach full field before the outgoing beam arrives 700 nsec later. The kickers deflect the outgoing beams approximately 1.2 mrad, sending them off toward water-cooled aluminum dumps. The space between quadrupoles Q18 and Q19 (≈ 11 m) accommodates the dc septum magnet. Quadrupoles Q17 and Q18, through which the outgoing beam must pass off-axis, are both horizontally defocusing and thus assist in extracting the beam rapidly.

4.4 The Chromatic Correction Section

The next two half-wave modules, used for the chromatic correction system, each have unity magnifications in the x and y planes. These modules each consist of an array of four identical quadrupoles with alternating polarities interspersed with sextupoles in a sequential symmetry arrangement. Dipoles were introduced at the junctions between the modules to produce a symmetric momentum dispersion about the center of this section. The first and third dipoles are of the same strength; the second dipole, located at the center, has twice the strength of the others. The sextupoles are connected in pairs at corresponding locations in the two modules, such that the momentum dispersion is the same at each member of the pair. Similarly, the R_{12} and the R_{34} matrix elements, the sine-like functions, have the same magnitude but opposite sign at each member of a given sextupole pair. This arrangement results in a natural cancellation of certain second-order aberrations, as discussed in Section 3.2 above. The strengths of the sextupole pairs were adjusted to minimize the dominant second-order chromatic aberrations, T_{126} and T_{346} of the combined CCS and final telescope system.

4.5 The Final Bend

The last dipole of the chromatic correction section, which provides the final bend before the IP, was actually built as two separate magnets, designated the "hard bend" and "soft bend" magnets, mounted end-to-end and powered in series. The hard bend, with a field of 12.5 kG, bends the beam through an angle of 17.3 mrad. The soft bend, 4.0 m long but with a field of only 417 Gauss, bends the beam through the last 1.00 mrad. This arrangement was included to reduce the critical energy of the synchrotron radiation that reaches the detector. The critical energy is given by

$$k_c = \frac{3}{2} \frac{\gamma^3}{\alpha} \frac{r_e}{\rho} m_e c^2$$
$$\approx 0.666 \text{ (MeV)} \left[\frac{E}{100 \text{ GeV}} \right]^2 B(\text{kG}) \tag{35}$$

where ρ is the radius of the bend and E is the beam energy in GeV. The hard-bend synchrotron radiation, with a critical energy of 2.08 MeV for a 50 GeV beam, is 29 mm from the beam at the entrance to the final triplet and can thus be masked off with a simple collimator. The soft-bend radiation which unavoidably passes into the detector, has a critical energy of about 69 keV.

A novel feature of the SLC final focus not found in conventional storage rings is the S-bend geometry formed by the antisymmetric bends of the north and south chromatic correction sections. Specifically, the final dipoles on the north side bend the electron beam to the west, while the final dipoles on the south side bend the positron beam to the east. This is illustrated in Fig. 10. This feature has been incorporated in the hope of further reducing the synchrotron radiation background in the experimental detector.

In a conventional storage ring, most of the dipole synchrotron radiation from both directions can be blocked by a pair of circular masks, symmetrically arranged on each side of the detector. Unavoidably, however, some of the radiation passing through the center hole of the first mask will strike the inside (detector side) surface of the second mask and back-scatter into the detector. With the beam energies and intensities planned for the SLC, these hot spots on the inside surfaces of the masks could be troublesome sources of hard x-ray background.

This problem can, in principle, be curtailed by introducing the S-bend. With this arrangement, the synchrotron radiation from the electron beam (approaching from the north) is all in a thin horizontal sheet to the east of the beam itself. The radiation from the positron beam is all in a horizontal sheet to the west. Masks with open slots on one side can then be arranged anti-symmetrically to block the incoming radiation but pass the outgoing radiation from the other beam. Whether or not this feature of the S-bend geometry will make a significant improvement in the overall background problem has yet to be verified.
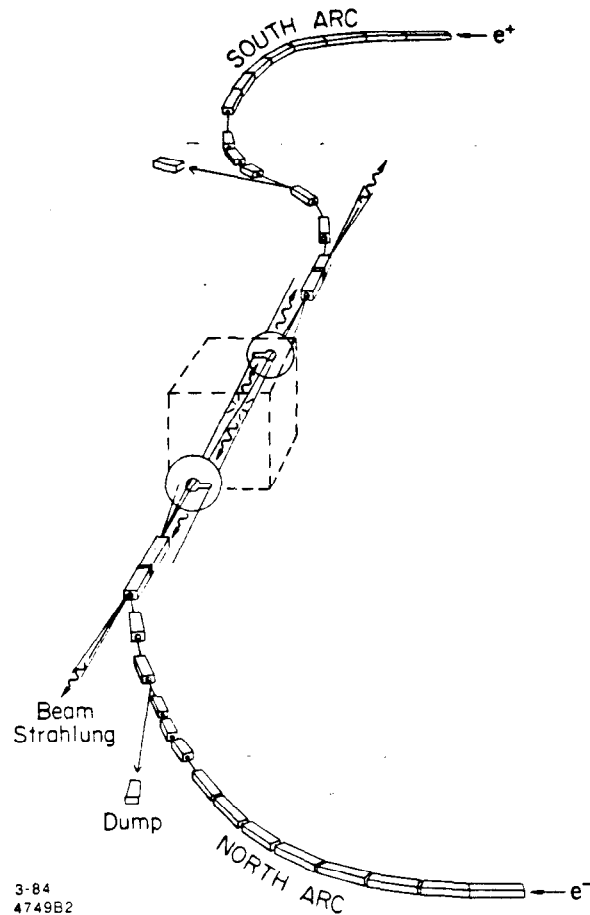
Fig. 10. The final bend configuration in the SLC. All bend angles are exaggerated in this figure.

4.6 The Final Telescope

The function of the final telescopic module is to focus the beam to the smallest possible spot size at the interaction point with equal demagnification factors in the x and y planes. In general, the higher the field gradient in the final quadrupole triplet, Q1, Q2, Q3, and the shorter the distance, ℓ^*, from the IP to the face of the first quadrupole, the smaller is the achievable beam spot and the higher the luminosity. As discussed in Section 4.1, two designs for the final telescope have been developed: one based on conventional iron quadrupoles, the other on high-gradient superconducting quadrupoles.

During the design of the final telescope, the first parameter to be frozen was its overall length, the distance between the interaction point and the waist in the beam envelope one-half betatron wavelength upstream. This distance was chosen somewhat arbitrarily to be approximately 38 m, based on general optical considerations and site boundary constraints. Studies demonstrated that a wide variety of telescope designs were possible using conventional, superconducting or permanent magnet[17] quadrupoles, all constrained to this total length.

Choosing the drift distance ℓ^* from the face of the innermost quadrupole to the interaction point required a compromise between the ultimate luminosity and the space requirements of the detector. For the design using conventional quadrupoles, this distance was chosen to be 2.82 m, the minimum consistent with avoiding any adverse saturation effects of the Mark II solenoid field on the field quality of the nearest quadrupole. At this distance, the stray solenoid field decreases to about 10 Gauss. The use of the conventional triplet at this ℓ^* is not compatible with the SLD detector, however, because of mechanical interference and because of the strong solenoid field extending out to about 4 m. The design using superconducting final triplets is based on an ℓ^* of 2.21 m. This was deemed to be the shortest ℓ^* that still allows room for beam position monitors, synchrotron radiation masks, and a precision vertex detector. The superconducting quadrupoles, cryostat, and SLD detector are outlined in Fig. 11. The conventional quadrupoles and the Mark II detector are indicated by dashed lines.
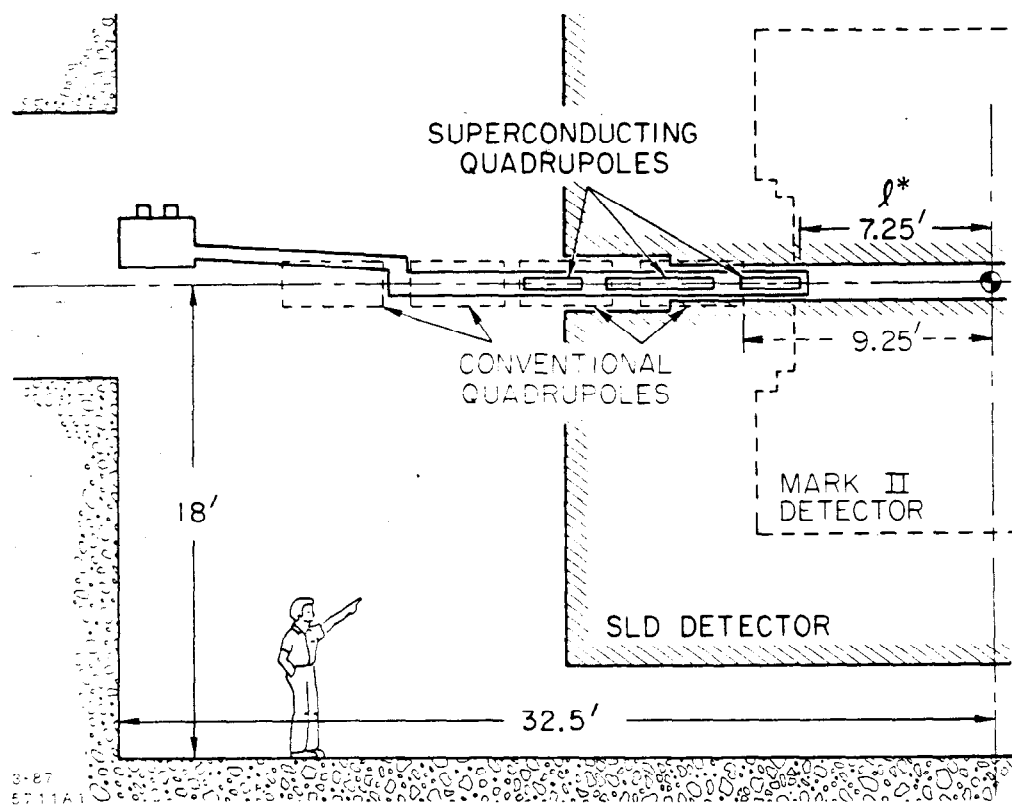

Fig. 11. Elevation view of the SLC interaction region showing the conventional quadrupoles and Mark II detector (dashed lines) with the superconducting quadrupoles and SLD detector superimposed.

The next step was to select the highest practical magnetic field gradient for the final quadrupole triplet. For the conventional iron quadrupoles, the pole-tip field was conservatively chosen to be 10 kG (at 50 GeV) to ensure against any magnetic saturation effects detrimental to the quality of the pure quadrupole field. For a given pole-tip field, the maximum gradient

that can be achieved in a quadrupole depends on its aperture. In this triplet, the minimum aperture required is determined primarily by background considerations. Off-axis electrons originating from beam-gas interactions and slit scattering upstream follow trajectories that reach their maximum excursions in the final triplet. Computer simulations indicated that a clear aperture of about 40 mm is necessary in this section to avoid an intolerable flux of secondary particles scattering into the experimental detector. Studies also showed that when the SLC reaches its full performance specifications, beam-beam disruption effects will generate an intense beacon of electromagnetic radiation out to an angle of about 2 mrad. (See Section 5.4 below.) An unobstructed path for this radiation requires a minimum aperture of about 35 mm. Subject to this constraint, a pole-tip gap of 1.625 inches and a gradient of 4.85 kG/cm were chosen for the conventional quadrupoles at 50 GeV. This gradient can be increased for beam energies up to at least 55 GeV before saturation effects become significant.

A gradient of 12 kG/cm has been chosen for the superconducting quadrupoles at 50 GeV. The aperture, measured to the innermost surface of the conductor, was chosen to be 2 inches, a practical lower limit imposed by the geometry of the keystone-shaped superconducting cable.[18] Allowing space for an inner helium passage and for the beam pipe, the clear aperture is about 40 mm, a value consistent with the other requirements discussed above.

Prototype magnets with these characteristics have been tested at Fermilab to gradients of over 18 kG/cm at 4.2° K. When installed in the SLC, the maximum attainable gradient will be lower than the test value, due to the external 6 kG detector solenoid field and to a higher and more economical operating temperature of 4.6° K (each causing about a 6% reduction in the maximum current). When tuned for 55 GeV, these quadrupoles will be running at about 80% of the quench limit.

Each quadrupole triplet is powered as a series string by a single power supply. Thus, the field gradient is the same in each member of each triplet. The quadrupoles of the conventional final triplet have separate trim windings with individual power supplies. These trims correct for fabrication errors and allow separate adjustment of the focal lengths in the horizontal and vertical planes. The superconducting quadrupoles do not have separate trim windings. Instead, the trim functions will be performed by bucking or boosting the triplet current with small supplies connected across each individual quadrupole.

The desired quarter-wave focusing properties of each triplet were obtained by adjusting the length and spacing of the magnets and the length of the middle magnet relative to the first and third (which were constrained to be identical to preserve the symmetric triplet properties). With ℓ^*, the total length, and the gradients of the final triplet quadrupoles fixed, and with the additional constraint that the system as a whole must preserve half-wave telescopic properties in both dimensions, the lengths and spacings of the final triplet quadrupoles and the overall strength

and spacings of the upstream triplet were varied to obtain the desired demagnification. Note that in the conventional configuration, Q2 is actually two magnets mounted closely together, as evident in Figs. 8 and 11, rather than a single long magnet. Splitting Q2 in this way was done to simplify fabrication and improve mechanical stability.

The "sliding telescope" property discussed in Section 2.4 was used to advantage in this part of the design to increase ℓ^* and at the same time to shorten the overall length of the telescope. In the superconducting design, for example, ℓ^* at 2.21 m is about 20 cm longer than the effective focal length of the final triplet alone, while the distance between the soft-bend dipole and Q6, and thus the total length of the telescope, is about 5 m shorter than it would have been with the simplified configuration of Fig. 4.

For a fixed total demagnification, the magnitudes of the sextupole fields in the chromatic correction section and, by implication, the severity of the uncorrected aberrations, grow as the final triplet strength is reduced. Demagnification factors (1/M) of 4 and 5 were chosen for the conventional and superconducting configurations, respectively. These magnifications are "diminishing returns" points in each case. Attempts to reduce the spot sizes by choosing stronger demagnifications were offset by increasing third-order aberrations.

The optimum configurations using conventional and superconducting final triplets do not have identical upstream triplets. However, a pair of solutions was found in which the same upstream magnets, Q4, 5, 6 can be used by adjusting their locations and field strengths.

An unusual feature of the SLC is the use of an anti-symmetric optical arrangement across the IP.[19] This was adopted to improve the masking of synchrotron radiation background originating in the final triplet quadrupoles. This is the quadrupole analog of the S-bend scheme described above for masking dipole radiation. The synchrotron radiation from the quadrupoles is generated in an elliptical pattern. By choosing the polarities to give the triplet on the electron side a focus-defocus-focus configuration while the positron triplet has a defocus-focus-defocus configuration, the major axes of the synchrotron light beams will be oriented horizontally on one side and vertically on the other. Elliptical masks with the same aspect ratio but rotated 90° with respect to the incoming radiation pattern will block much of the incoming radiation, while allowing outgoing radiation (that which passed the mask on the incoming side) to pass out of the detector without back-scattering.

4.7 Expected Performance

Figure 12 shows horizontal and vertical betatron functions (β_x and β_y) for the final telescope. The solid lines show these functions for the superconducting quadrupoles. The dashed lines show these functions for the conventional triplet configuration.
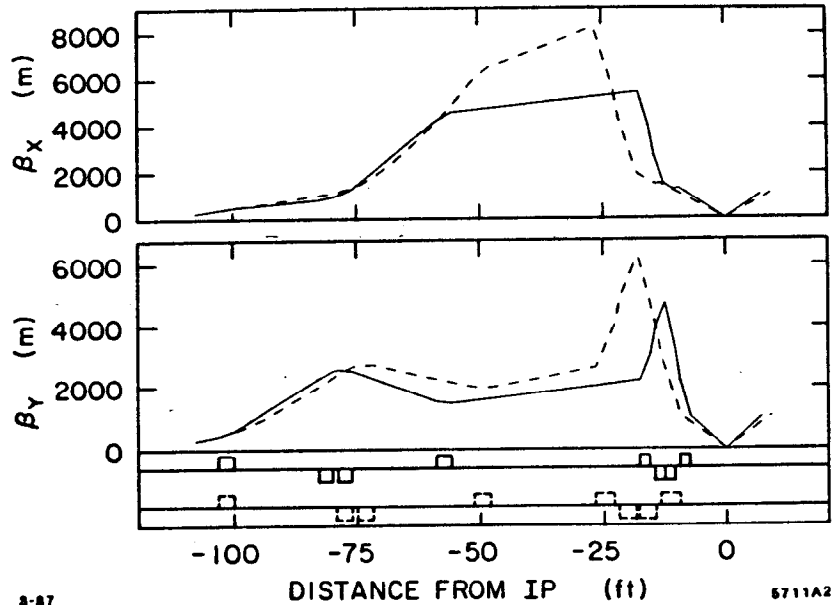
Fig. 12. Horizontal and vertical beta functions in the final telescope. The solid lines indicate the superconducting configuration; the dashed lines indicate the conventional configuration. The positions of the quadrupoles are shown along the bottom of the figure.

The main differences between the conventional and superconducting configurations are summarized in Table 1. The spot size listed is the rms radius (σ) of the beam at the interaction point,

Table 1. Parameters for the two final focus configurations at 50 GeV.

	Initial	Upgraded	
Quadrupoles	Conventional	Superconducting	
Clear Aperture	3.95	4.13	cm
Gradient	4.85	12.0	kG/cm
Drift Length (ℓ^*)	9.25	7.25	ft.
Demagnification	$\times\,4$	$\times\,5$	
β^*	0.75	0.50	cm
First Order Focus	1.5	1.2	μm
Spot Size (σ^*)	2.07	1.65	μm
Repetition Rate	120	180	$\sec^{-1}$
Particles/Bunch	5×10^{10}	7.2×10^{10}	$N^{\pm}$ /bunch
Emittance at IP	4.2×10^{-10}	4.2×10^{-10}	$\varepsilon_{x,y}$ (rad m)
Disruption Parameter	0.34	0.76	D
Pinch Factor	1.14	2.2	H
Luminosity	6.4×10^{29}	6.0×10^{30}	$cm^{-2}\ sec^{-1}$

26

including residual aberrations. For low beam currents, the luminosity is inversely proportional to σ^2; thus, the superconducting configuration is expected to yield at least 1.6 times greater luminosity than the conventional. Note that the "Upgraded" column also shows planned improvements in the repetition rate and in the number of particles per bunch, which contribute factors of 1.5 and 2, respectively. In addition, as the number of particles per beam pulse is increased, this relative luminosity gain is expected to increase further, multiplied by a "pinch factor" due to the beam-beam disruption effect. This would enhance the luminosity by an additional factor of 2 for the full design current.[1]

5. TUNING AND DIAGNOSTICS

The tolerable errors in the positions and strengths of the magnetic elements of a final focus system may be very small, depending on the amount of demagnification, the absolute size of the beam, and other factors. The alignment tolerance on the last focusing element, for example, must be less than σ^*, and the tolerance on the strength must be small enough that $\Delta f \ll \beta^*$, if the resulting loss of luminosity is to be negligible.

In the SLC, the position of the final quadrupole triplet must be held stable to about 1 μm, and the field strengths must be controlled to the level of 1 part in 10^4. Calibrating the absolute strength of an iron-core quadrupole to an accuracy of 1 part in 10^4 is a formidable task requiring careful attention to end-field effects, hysteresis, core temperature and the measurement of the excitation current. Achieving the necessary accuracy for all components of a large system directly by careful construction is impractical for any plausible collider design.

In practice, a final focus system must be instrumented to monitor the position and size of the beams at critical points, and procedures must be available to use this information to diagnose the problems that arise from any deviations from design specifications. Controls must then be provided to correct for steering and optical errors. These may be implemented with trim windings on the main magnets, special "corrector" dipoles and quadrupoles, or remotely controlled mechanisms for moving critical focusing elements.

5.1 Tuning the SLC

Tuning the final focus of the SLC is done in several steps.[20] The first step is simply to steer the beams through the system to their respective dumps. This is done with pairs of small vertical and horizontal dipoles distributed throughout the final focus system, at least one pair per quarter-wavelength of betatron phase. This steering is guided by strip-line Beam Position Monitors (BPMs), one adjacent to each sextupole in the chromatic correction section, and one or two per triplet in the other sections. In the SLC, this steering can be done to an accuracy of about 100 μm at each BPM.

In a simple optical telescope like the one in Fig. 4, there is a one-to-one correlation between the location of the last lens and the image point. This is also true for the final telescope of the SLC. Moving the final triplet 1 μm transversely moves the focused beam spot 1 μm. At this level, temperature variations in support structures and floor movements due to ground settling become important.

Movements of a few microns can be compensated with small steering dipoles immediately upstream of Q3. Larger dipole corrections are undesirable at this point, however, because the resulting large betatron oscillations that result from an off-axis trajectory through the triplet generate linear dispersion, increased synchrotron radiation, and possible geometric aberrations from imperfections in the quadrupole fields. In the SLC, these problems are avoided with a remotely-controlled motorized support system that allows the final triplet to be moved over a range of about ± 2 mm with a step size of about 10 μm.

After the beam trajectories have been centered in all the quadrupole apertures, the residual dispersion is corrected. This dispersion is measured by observing beam centroid shifts in each of the BPMs as the incoming beam energy is varied and comparing to the nominal design values. Corrections are made using four small quadrupoles near B5 and B6 in the η-matching section (Fig. 8), two upright quads which couple mainly to η_x (near B5) and η'_x (near B6), and two skew quads which couple mainly to η_y and η'_y. An automated procedure has been developed to measure and correct the residual dispersion in a few seconds.

The amplitude and phase of the betatron oscillations in the chromatic correction section and final telescope can be adjusted with the quadrupoles in the upper transformer, each of which has a separate power supply to facilitate these adjustments. When the betatron phase is properly adjusted to center the waist in B3, quadrupoles Q16 and Q17 can be used as a zoom lens to adjust the magnification.

Because of the roll variations introduced by the terrain-following feature of the SLC, small alignment and magnet setting errors tend to introduce coupling between the x and y components of the beam parameters. This coupling typically enlarges the beam size along the diagonal direction. Skew quadrupoles were introduced near Q3 and Q17 to untangle this coupling. They are symbolized by diamonds in Fig. 8. The effect of the skew quad near Q17 can be seen on a profile monitor in the high-β region near Q4. This skew quad is adjusted to rotate the elliptical beam spot upright. The skew quad near Q3 is used to remove any remaining xy coupling, including the coupling introduced by the solenoid field of the experimental detector. This skew quad can only be adjusted by observing the final spot size at the IP, or some direct manifestation of the small spot size, as discussed below.

The final focusing of the beam at the IP is done with small adjustments to the strengths of Q2B and Q3. These two magnets, adjusted in combination, move the x-waist and y-waist

along the z-dimension to bring them together at the collision point. Like the last skew quad adjustment, this can only be done by observing the properties of the beam at the IP. Ultimately, some observable quantity related to luminosity, a figure of merit for the performance of the machine, must be available to guide in tuning the machine.

5.2 Luminosity Monitoring

The e^+e^- elastic scattering ("Bhabha" scattering) rate has been a useful figure of merit for conventional storage rings. The Bhabha rate can be calculated from fundamental principles with high accuracy and thus gives an absolute measure of luminosity. The scattering rate into an angular region bounded by θ_{min} and θ_{max} is $R = \mathcal{L}\Delta\sigma$, where

$$\Delta\sigma = \frac{4\pi\alpha^2}{E^2}\left(\frac{1}{\theta_{min}^2} - \frac{1}{\theta_{max}^2}\right) \tag{36}$$

is the Bhabha cross section, E is the energy of each beam, and α is the fine structure constant. It is interesting to note that the Bhabha scattering rate will be the same for any e^+e^- collider having the luminosity and energy relationship of Eq. (2).

The small-angle-monitor ("SAM") built for the Mark II detector at the SLC is an array of detector elements designed to identify back-to-back e^+e^- pairs scattered into an angular range from 50 to 150 mrad of the beam direction. At a luminosity of 10^{30} cm^{-2} sec^{-1} and 50 GeV per beam, a detectable Bhabha rate of 0.014 events/sec is expected. Mini-SAM, a device that covers the region from 15 to 25 mrad to supplement the SAM measurements, will raise the total detected Bhabha rate to 0.32 events/sec. The usefulness of the mini-SAM will depend on its ability to distinguish Bhabha scatters from off-axis background particles. Assuming this can be done successfully, a 10% measurement of luminosity will require 100 counts and will take about five minutes at this rate with the combined data of SAM plus mini-SAM. With the SAM alone, this measurement will take about two hours. Starting in an untuned condition with a luminosity of, say, 10^{27} cm^{-2} sec^{-1}, a single 10% measurement with the combined SAM/mini-SAM system will take 3.6 days.

The conclusion to be drawn from this is that Bhabha scattering may be useful for charting the integrated luminosity and normalizing large blocks of experimental data but is far too slow to be of any value in guiding any beam-tuning procedures.

5.3 Profile Monitoring Devices

Profile monitors based on a fluorescent screen in the path of the beam, viewed by a TV camera, have proven to be immensely valuable at many places in the SLC including the interaction point. They have been used for diagnosing hardware problems, verifying the proper operation of magnets,

measuring emittance, and tuning out cross-plane coupling. Resolutions of 50 μm are routinely achieved, and the prospect of reaching 10 μm resolution with this technique seems likely. Beyond this point, the diffraction limits of camera lenses and the graininess of fluorescent screens become important.

Another approach to monitoring small spot sizes is based on detecting the secondary emission signal generated when the beam is scanned across a thin carbon fiber. A device using fibers as small as 4 μm in diameter has been in use at the interaction point during the commissioning tests of the SLC. Figure 13 shows a 5.2 μm beam profile measured with a carbon fiber. This particular measurement was significant because it marked an official milestone in the SLC commissioning: it was the first beam spot smaller than 6 μm.

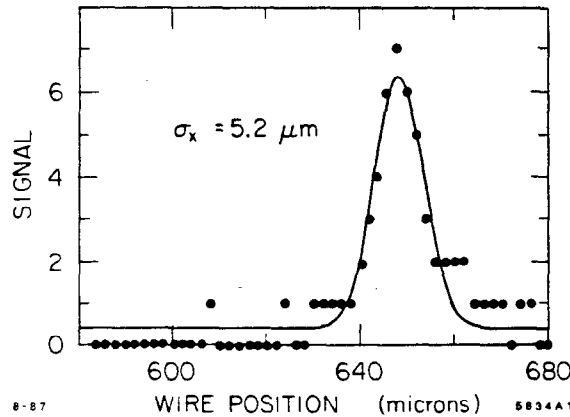Fig. 13. Electron beam profile measured at the SLC interaction point using a 7μm diameter carbon fiber.

An important limitation on the usefulness of the wire scanning technique is the survivability of the fiber when blasted by the charged particle beam. Fibers of various sizes up to 25 μm diameter have been used successfully for many hours in the SLC with no evidence of beam-induced failure, but only at a low bunch population ($\leq 5 \times 10^9$ particles/bunch) and low repetition rate (5 pps). The fibers are not expected to survive with SLC design-spec beams.[21] It will be necessary to focus the machine at reduced beam current and then increase the current only after the fibers are moved safely to the side, clear of the beam. In future colliders with smaller spot sizes and higher bunch densities, wire scanners may prove useful in performing the functions now performed by fluorescent screens in the SLC, but for final adjustments at the interaction point a different technique will be needed.

5.4 Beamstrahlung Radiation

Beamstrahlung is the name given to the radiation emitted by each bunch as it passes through the electromagnetic field of an opposing bunch. The radiation emitted by a particular particle depends on the net force it feels in this passage. The maximum radiation is emitted by particles

offset about 1.5 σ from the center. In contrast, the maximum contribution to the luminosity comes from particles at the center of the bunch, where they are most likely to collide with particles of the opposing bunch.

When two Gaussian bunches collide, the fraction of one bunch's energy radiated away is given approximately by the classical synchrotron radiation formulation:

$$\delta_c = \frac{r_e^3 N^2 \gamma}{3\sqrt{3} \, \sigma_z \, \sigma_r^2} \tag{37}$$

where σ_z and σ_r are the longitudinal and radial sizes of the bunches, N is the number of particles in the "target" bunch, r_e is the classical radius of the electron, and $\gamma = E/m_e c^2$. For equal size opposing beams, the number of photons emitted is proportional to $1/\sigma_r$, and the critical energy of the radiation spectrum is also proportional to $1/\sigma_r$. The radiation is peaked strongly forward in the direction of the beam motion.

Beamstrahlung radiation is a macroscopic manifestation of beam-beam interactions that can, in principle, be detected and quantified for each collision. While it is not strictly proportional to luminosity, the beamstrahlung flux above a given threshold is an observable quantity that generally increases with luminosity as the beams are brought into focus. In the SLC design, this radiation is intercepted by special detectors[22] located along a line-of-sight from the IP, just upstream of the last large dipole bending magnet on each side as shown in Fig. 10. The expected performance of the SLC beamstrahlung system is shown in Fig. 14.

The small spot and high luminosity parameters of the TeV class collider studies lead to beamstrahlung fluxes that carry off a substantial fraction of the total beam energy. These machines enter the quantum beamstrahlung regime, where the classical synchrotron radiation formula is no longer adequate. Himel and Siegrist have shown[23] that in this regime, the fraction of the beam energy radiated is proportional to $\sigma_r^{-2/3}$. As in the classical regime, tuning for maximum beamstrahlung will generally maximize the luminosity.

6. STEERING TO COLLISION

In an e^+e^- storage ring with a purely magnetic guide field, the counter-rotating beams follow exactly the same central trajectory and thus head-on collisions are unavoidable. There is no *a priori* reason why this should be true in linear colliders, however. In any linear collider, including the SLC, the opposing beams must be actively steered into collision, guided by some observable that is sensitive to the impact parameter. Using state-of-the-art strip-line BPMs, it may be possible to direct the two beams independently to the intended interaction point with an accuracy of perhaps 100 μm. In order to achieve useful luminosity, the beams must be steered to within about one beam radius of each other. This corresponds to about 2 μm in the SLC and is likely to
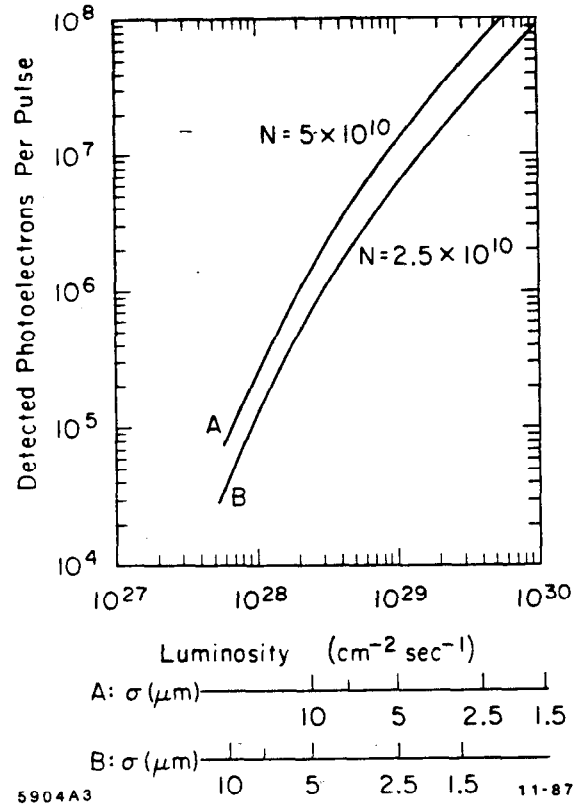
Fig. 14. Predicted signal strength in the SLC beamstrahlung monitor increases monotonically with luminosity for identical round beams.

-be much smaller in a TeV-class linear collider. It is in this regime, far below the resolution limits of single-beam diagnostic devices, that the beam-beam deflection is strongest.

6.1 Beam–Beam Deflections

The electromagnetic force acting between two intense colliding beams of oppositely charged particles will cause them to be deflected in passing by an angle that depends on the offset between the bunches and the distribution of charge within the bunches. This is illustrated in Fig. 15. This deflection, measurable with nondestructive techniques, is expected to be the key to the final steering of the e^+e^- beams in the SLC.[24] Furthermore, this deflection is expected to be a measurable manifestation of the interactions between even the extremely small beams envisioned for a large future linear collider.

The deflection of a single particle of charge e, passing at an offset Δ from the centroid of an oppositely charged Gaussian distribution, is given by:

$$\theta(\Delta) = \frac{-2r_e N_T}{\gamma} \frac{1 - \exp[-\Delta^2/2\sigma^2]}{\Delta} \quad , \tag{38}$$
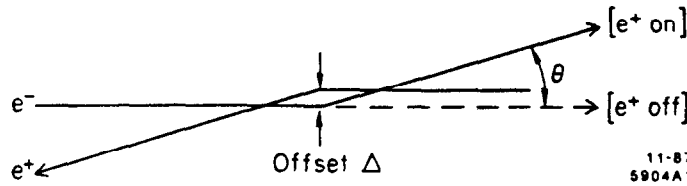
32

Fig. 15. The trajectory of each beam is deflected by the opposing beam passing at
an offset $\triangle$. The dashed line shows the trajectory followed by the e^- beam when
the e^+ beam is suppressed.

where r_e is the classical radius of the electron, N_T the number of particles in the target bunch
and σ the RMS transverse size of the Gaussian distribution.

When two beams pass with offsets large compared to their transverse sizes, they see each
other as point charges and Eq. (38) is a good approximation for their mutual deflection. When
colliding with a small offset, the finite sizes of the beam distributions must be taken into account.
This can be done by convoluting Eq. (38) with the distribution of the opposing beam. The result
of such a calculation, carried out in the limit of small $\triangle$, is expressed in terms of a form factor[25]
which reduces the average deflection:

$$F(R) = \frac{\ell n(1 + R^2)}{R^2} \ . \tag{39}$$

Here R is the ratio of the transverse sizes of the two beams.

6.2 Application to the SLC

Deflection versus offset is plotted in Fig. 16 for 50 GeV beams consisting of 5×10^{10} particles,
with transverse spot sizes σ of 2, 5 and 10 μm. 10 μm is the typical size of the beams at the SLC
interaction point after beam steering and dispersion corrections have been made but before optical
corrections are completed. Magnet setting errors and misalignments contribute to this estimate.
By adjusting the final focus corrector magnets and quadrupole trims, σ can be reduced to about
2 μm. The form factor described above has been incorporated in the curves as a multiplying
reduction factor, assuming in each case $R = 1$.

Several methods have been studied for detecting and measuring the beam-beam deflections.
The most obvious is to use a pair of BPMs straddling the interaction point. If the drift length
"lever arm" is long enough, a deflection at the IP will result in a measurable position shift at the
BPM. The power of this method can be greatly enhanced by suppressing the opposing beam on
some pulses and watching the measured beam jump back to its undeflected position. To make
this possible, a pair of pulsed magnets, the "single-beam dumpers," have been provided to kick
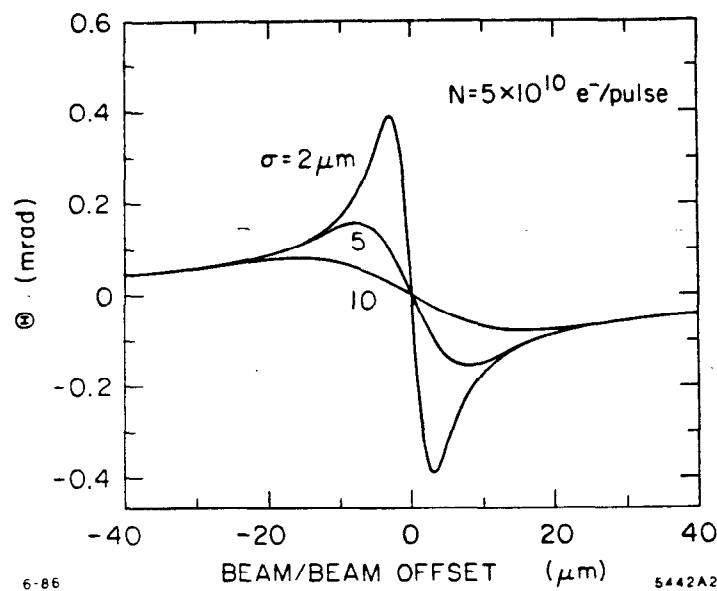either beam out of the transport system on command. These are shown in Fig. 17.

Fig. 16. The deflection angle θ as a function of offset $\triangle$, plotted for three spot sizes.

Another approach is based on detecting beamstrahlung radiation. The angular distribution of the beamstrahlung photons, strongly peaked forward in the direction of the outgoing beam and undeflected by intervening magnets, can be measured with a segmented detector with the arrangement described in Section 5.4 above.

Yet another approach is to observe the sizes and positions of the outgoing beams after they have been extracted from the main transport system but before they reach the dumps. The long lever arm from the IP to the dump on each side of the SLC makes the beam position at this point sensitive to the angle at the IP. Furthermore, destructive monitoring devices, such as fluorescent screens, can be left in place at the dumps without interfering with the incoming beams.
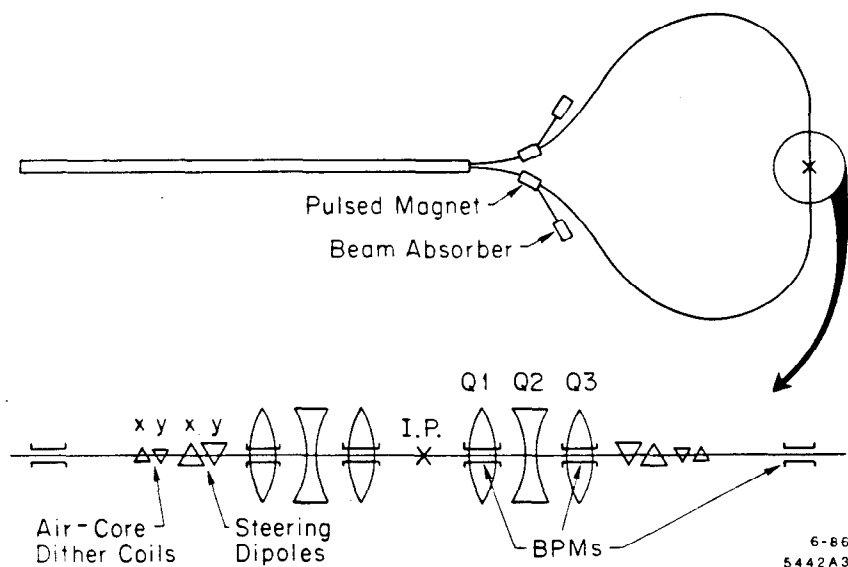

Fig. 17. Schematic of beamline components relevant to the deflection technique.

The procedures described here are based on relative measurements of the outgoing beam position at locations where the angular deflection produced in the collision leads to a transverse position shift. There are several BPMs in the outgoing transport system of the SLC that are suitable for this purpose. The best locations, however, are in the final telescope quadrupoles where the β-functions reach their largest values, thereby magnifying the deflections the most, and where dispersion is negligible, (which minimizes confusion with energy variations). These locations are indicated in Fig. 17.

A three-step tuning procedure is envisioned:

1. Initial beam finding: One beam — designated the "target" in this case — is momentarily suppressed with a single-beam dumper while position measurements are made on the "probe" beam. In this way, the shift induced by the target beam can be determined. When the offset between the beams is large, the magnitude of the shift is inversely proportional to the offset, and its sign tells in which direction to steer. This can be seen by taking the limit of Eq. (38) for large $\triangle$:

$$\theta(\triangle) \simeq \frac{12 r_e \, N_T}{\gamma} \, \frac{1}{\triangle} \, . \tag{40}$$

The useful range of this technique, i.e., the maximum offset that still gives a measurable deflection, is limited only by the ability of the BPMs to resolve beam centroid movements. For example, assume the BPM near the innermost quadrupole in the SLC can resolve the centroid position of a single bunch of 5×10^9 particles to a level of 20 μm. It will then be possible to detect relative beam-beam offsets up to a maximum of:

$$\triangle(\mu\text{m}) \simeq 40 \, \frac{N_T}{5 \times 10^9} \, . \tag{41}$$

If the initial offset between the beams is too large to give a measurable deflection, the wire-scanning technique described in Section 5.3 can be used to bring both beams within a fiber-width of each other. Notice, however, that this "capture range" drops as $1/E$. For a larger collider with ten times the energy but the same N_T and BPM arrangement, the beams will have to be steered to within 4 μm of each other before the deflection can be detected. If this can not be done with a wire scanner or other direct means, an automated "raster scan" could be used to search a small area, scanning one beam while looking for deflections of the other. For larger beam currents, it may be possible to do better than the limit indicated in Eq. (41), because the BPM resolution also improves with increasing current. By chopping one beam off and on and averaging over many pulses, the resolution can be improved further.

2. Beam centering: Scanning the target across the probe and recording a plot similar to Fig. 15 for the probe will facilitate optimal steering of the two beams. The zero-deflection symmetry point is reached when the beams are perfectly centered.

3. Spot size tuning: Taking the limit of Eq. (38) for small $\triangle$ and multiplying by the form factor (39) gives:

$$\theta(\triangle) \simeq \frac{-r_e \, N_T}{\gamma} \frac{\triangle}{\sigma^2} F(R) \quad . \tag{42}$$

The slope of the deflection of the probe beam near the zero-deflection symmetry point is inversely proportional to the cross-sectional area of the target. By differentiating Eq. (38), it can be seen that the deflection is maximum for offsets of about 1.6 standard deviations of the target distribution, and that the maximum deflection scales as the inverse of the transverse spot size:

$$\theta_{\max} = 0.451 \frac{2r_e \, N_T}{\gamma} \frac{1}{\sigma} \quad . \tag{43}$$

A relative measure of spot size can thus be obtained by scanning one beam across the other as in Step 2 above. Guided by these measurements, an operator can adjust optical elements of the transport system to minimize this final size.

6.3 Maintaining Collisions

It is expected that even when the static crossing errors have been corrected as described above, the two beams will not remain centered on each other without an active feedback system. Many sources of drift and jitter that could cause the beams to wander at the IP have been identified at the SLC. In most cases, these effects can be minimized with careful attention to hardware designs. Magnet power supplies, for example, must be well-regulated, and support structures must be rigid. Natural ambient ground vibrations at frequencies above 1 Hz have been shown[26] to be negligible at the level important for the SLC, although some local man-made vibration sources, such as reciprocating pumps, require special isolation. On a slower time scale, thermal effects will cause mechanical support structures to expand and power supplies to drift enough to adversely affect the luminosity unless steering corrections are made. Studies of feedback schemes for the SLC have focused on simple and relatively slow algorithms, although the BPM electronics, control system and other key components have been built to allow pulse-by-pulse feedback to accommodate faster or more complex schemes.

A simple feedback algorithm for correcting relatively slow drifts is based on automatically suppressing one beam periodically using a single-beam dumper, while observing the motion of the other beam. Of course, luminosity would be sacrificed on these occasional pulses, but they would enable a steering correction to be computed from the measured position shifts of the outgoing beam. Because each measured deflection can correspond to two possible offsets, the operation

has to be carried out frequently enough to ensure that the actual offset does not drift outside the domain of the IP, bounded by the deflection maxima, in the time between updates. This technique is adequate to track the thermal expansion of support structures and other mechanical effects in the SLC.

An approach that does not require sacrificing any beam pulses would be to excite small "dither coil" dipoles (Fig. 17) in a preprogrammed way to induce small periodic offsets at the IP with an amplitude of a fraction of a standard deviation. In this way, one beam can be made to trace out a pattern such as a small circle at the IP. The deflections of the opposing beam will then project the same pattern at the BPM. When the offset between the beams corresponds to a point on a steeply rising positive slope in Fig. 16 (beyond the 1.6 σ peak on either side), the projection is a magnified image of the dither pattern. When the offset is less than 1.6 σ, the projection is an inverted image of the dither pattern. Synchronous position measurement would then allow a determination of whether the beams were colliding within or beyond 1.6 standard deviations of each other. If necessary, a correction could be applied to bring them back to within 1 σ. The sign of the deflection would indicate the direction in which to steer. In both these algorithms, corrections are applied using steering correctors immediately upstream of the final triplet.

ACKNOWLEDGEMENTS

REFERENCES

1. *SLC Design Handbook* (December 1984).

2. See, for example, B. Richter, *Very High Energy Colliders*, SLAC–PUB–3669 (May 1985) and *Proceedings of the 1985 Particle Accelerator Conference*, IEEE Trans. Nucl. Sci., NS–32 No. 5 (October 1985), 3828.

3. See, for example, the section on *Emittance Production and Preservation*, of the *Proceedings of the Symposium on Advanced Accelerator Concepts*, Madison, WI, August 1986, AIP Conference Proceedings 156 (1987).

4. R. Palmer, *Interdependence of Parameters for a 1-TeV Collider*, SLAC AAS Note-31 (May 1987).

5. R. Hollebeek, *The Linear Collider Beam-Beam Problem*, these proceedings.

6. See, for example, P. Chen, J. J. Su, T. Katsouleas, S. Wilks and J. M. Dawson, *Plasma Focusing for High Energy Beams*, IEEE Trans. Plasma Sci. PS-15 (1987) 218; and P. Chen, *A Possible Final Focusing Mechanism for Linear Colliders*, Particle Accelerators 20 (1987) 171.

7. K. L. Brown, F. Rothacker, D. C. Carey and Ch. Iselin, *TRANSPORT, A Computer Program for Designing Charged Particle Beam Transport Systems*, SLAC-91 (May 1977).

8. The subscripts 1 and 2 on x and θ are used in this paper to indicate the input and output, respectively, of a final focus system. Beware of possible confusion with the subscripts 1 through 6 of the x-vector and R matrix, which indicate the variables, e.g., $x_6 = \delta$.

9. *Proceedings of the SLC Workshop on Experimental Use of the SLAC Linear Collider*, SLAC-Report-247 (March 1982).

10. K. L. Brown, *A First- and Second-Order Matrix Theory for the Design of Beam Transport Systems and Charged Particle Spectrometers*, SLAC-Report-75 (June 1982).

11. J. J. Murray, K. L. Brown and T. Fieguth, *The Completed Design of the SLC Final Focus System*, SLAC-PUB-4219 (February 1987).

12. R. Hollebeek and A. Minten, *Disruption and Luminosity of Flat Beams*, SLAC CN-302 (1985).

13. A. Chao, J. Hagel, F. Ruggiero and B. Zotter, *A Flat Beam Final Focus*, CERN-LEP-TH/87-48 (September 1987).

14. D. C. Carey, K. L. Brown and Ch. Iselin, *DECAY TURTLE, A Computer Program for Simulating Charged Particle Beam Transport Systems, Including Decay Calculations*, SLAC-246 (March 1982).

15. R. Erickson, T. Fieguth and J. J. Murray, *Superconducting Quadrupoles for the SLC Final Focus*, SLAC-PUB-4199 (January 1987).

16. *SLD Design Report*, SLAC-273, (May 1984).

17. J. Spencer, *Some Optics Alternatives for the FFS*, SLAC CN-264 (February 1984).

18. R. A. Lundy, B. C. Brown, J. A. Carson, H. E. Fisk, R. H. Hanft, P. M. Mantsch, A. D. McInturff, R. H. Remsbottom and R. Erickson, *High Gradient Superconducting Quadrupoles*, IEEE Trans. on Nucl. Sci., NS-32, No. 5 (1985), 3707.

19. The anti-symmetrical optical scheme using elliptical masks was suggested by T. Himel.

20. P. S. Bambade, *Beam Dynamics in the SLC Final Focus System*, SLAC-PUB-4227 (June 1987).

21. C. Field, private communication.

22. G. Bonvicini, C. Field and A. Minten, *Beamstrahlung Monitor for the SLC Final Focus Using Gamma Ray Energies*, SLAC-PUB-3980 (May 1986), and *Proceedings of the 1986 Linear Accelerator Conference*, SLAC-Report-303 (September 1986).

23. T. Himel and J. Siegrist, SLAC-PUB-3572 (February 1985).

24. P. Bambade and R. Erickson, *Beam-Beam Deflections as an Interaction Point Diagnostic for the SLC*, SLAC-PUB-3979 (May 1986), and *Proceedings of the 1986 Linear Accelerator Conference*, SLAC-Report-303 (September 1986).

25. This parametrization was suggested by P. Bambade.

26. G. Bowden, *Mechanical Vibrations of the Final Focus*, SLAC CN-314 (1985); G. E. Fischer, *Ground Motion and Its Effects in Accelerator Design*, in Physics of Particle Accelerators, AIP Conference Proceedings 153, Vol. 2 (1987).